Electronic Supplementary Material (ESI) for Physical Chemistry Chemical Physics.

Particulate photocatalytic reactors with spectrum-splitting function for artificial photosynthesis

Yasuhiko Takeda,* Tomiko M. Suzuki, Shunsuke Sato, and Takeshi Morikawa

Toyota Central Research and Development Laboratories, Inc., 41-1, Yokomichi, Nagakute, Aichi 480-1192, Japan

*Corresponding author, takeda@mosk.tytlabs.co.jp

Supplementary Information

S.1 Impacts of material properties

The change in J_{sup} dependent on E_g and $\Delta\mu_{op}$ for the single-material reactor was investigated in detail, for interpretation of the impact of E_g deviation shown in Fig. 5. Figure S1 shows J_{sup}, qN_{rad}, and qN_{nonad} as functions of $\Delta\mu_{op}$ for the single-material reactor optimized for H_2 production. When $\Delta\mu_{op}$ is small, J_{sup} approximately equals qN_{abs}, and then starts to decrease owing to rapidly increasing qN_{nonad}. On the other hand, qN_{rad} is negligibly small leading to no impact on J_{sup} under the present condition. The optimal E_g is determined so that J_{sup} is slightly smaller than qN_{abs} at $\Delta\mu_{op}$ = 1.6 eV.

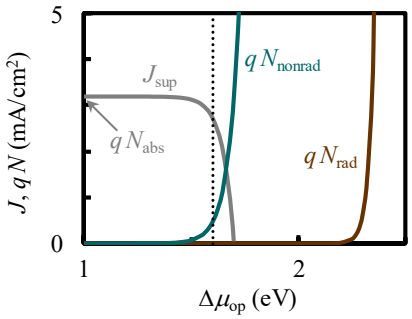

Fig. S1 Relations of J_{sup}, qN_{rad}, and qN_{nonad} vs. $\Delta\mu_{op}$ of the single-material reactor (E_g = 2.79 eV) for H_2 production ($\Delta\mu_{op}$ = 1.6 eV). m_c = 2 m_0, τ_{nonrad} = 1 ns, and w = 4 μm are adopted. The dotted line shows $\Delta\mu_{op}$ = 1.6 eV.

When E_g increases from the optimal value (2.79 eV), N_{abs} and consequently J_{sup} in the small $\Delta\mu_{op}$ range decrease, while J_{sup} is approximately constant up to a higher $\Delta\mu_{op}$, as depicted in Fig. S2. Therefore, J_{sup} at $\Delta\mu_{op}$ = 1.6 eV gradually decreases with increasing E_g. On the other hand, J_{sup} starts to decrease at a smaller $\Delta\mu_{op}$ when E_g is smaller. Therefore, J_{sup} at $\Delta\mu_{op}$ = 1.6 eV is dramatically lower.

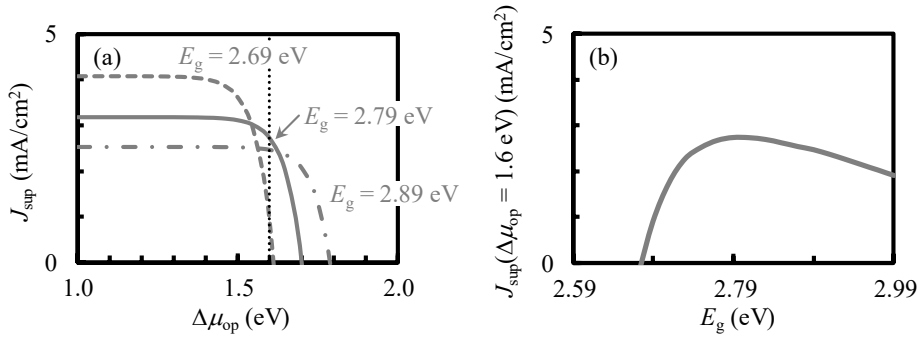

Fig. S2 (a) Relations of J_{sup} vs. $\Delta\mu_{op}$ of the single-material reactors with different E_g. m_c = 2 m_0, τ_{nonrad} = 1 ns, and w = 4 μm are adopted. (b) Dependence of J_{sup} at $\Delta\mu_{op}$ = 1.6 eV on E_g. The dotted line shows $\Delta\mu_{op}$ = 1.6 eV.

The relation of J_{sup} vs. $\Delta\mu_{op}$ is applied to solar cells. When a solar cell is combined with a power conditioner, E_g is optimized so that the output power density, P_{out} = $N_{sup}\Delta\mu_{op}$, is the maximal. The $\Delta\mu_{op}$ point at which P_{out} as a function of $\Delta\mu_{op}$ is the maximal, $P_{out}^{(max)}$, i.e., so-called the maximal power point shifts dependent on E_g, as shown in Fig. S3. However, the impact of E_g deviation on $P_{out}^{(max)}$ is extremely weaker than that on J_{sup} at a given $\Delta\mu_{op}$ for the photocatalytic reactors.

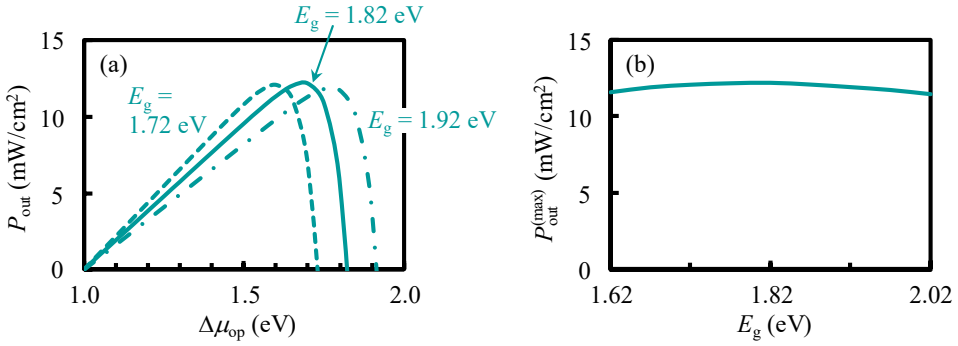

Fig. S3 (a) Relations of P_{out} vs. $\Delta\mu_{op}$ of single-junction solar cells with different E_g. m_c = 2 m_0, τ_{nonrad} = 1 ns, and w = 4 μm are adopted. (b) Dependence of $P_{out}^{(max)}$ on E_g.

When m_c is small and τ_{nonrad} is long, N_{nonrad} reduces proportionally to $m_c^{3/2}/\tau_{nonrad}$. The effect of the reduction in N_{nonrad} was investigated in detail. For example, the optimal E_g values in the WG-NG reactor for H_2 production are E_{gWG} = 2.30 eV and E_{gNG} = 1.82 eV at $m_c = 2\ m_0$ and τ_{nonrad} = 1 ns. The carrier supply rates of the WG and NG compartments (N_{WG} and N_{NG}) converted to the current densities as functions of $\Delta\mu_{op}$ are depicted in Fig. S4(a). The E_{gWG} and E_{gNG} are optimized so that N_{nonrad} is negligibly small and hence J_{sup} is approximately constant up to $\Delta\mu_{op}$ = 1.6 eV. When N_{nonrad} reduces at $m_c = 0.3\ m_0$ and τ_{nonrad} = 10 ns whereas E_{gWG} = 2.30 eV and E_{gNG} = 1.82 eV remain, J_{sup} is constant up to a higher $\Delta\mu_{op}$ of 2.2 eV, as shown in Fig. S4(b). Then, E_{gWG} and E_{gNG} are again optimized so that J_{sup} starts to decrease at around $\Delta\mu_{op}$ = 1.6 eV and instead N_{abs} is as large as possible. The results are shown in Fig. S4(c); $q N_{WG}$ and $q N_{NG}$ at a small $\Delta\mu_{op}$ increase owing to the narrower values of E_{gWG} = 2.04 eV and E_{gNG} = 1.52 eV. Consequently, J_{sup} at $\Delta\mu_{op}$ = 1.6 eV increase as depicted in Fig. 6(a).

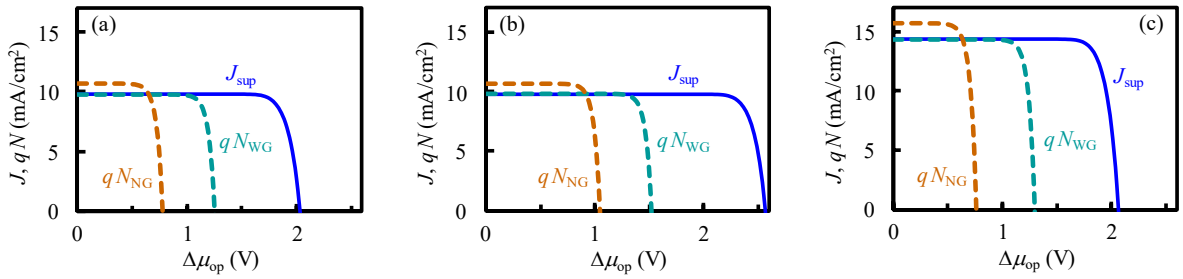

Fig. S4 J_{sup} vs. $\Delta\mu_{op}$ relations of the WG-NG reactor for H_2 production ($\Delta\mu_{op}$ = 1.6 eV), and $q N_{WG}$ and $q N_{NG}$ vs. $\Delta\mu_{op}$ of the WG and NG compartments. w = 4 μm. The following material parameters are adopted: (a) E_{gWG} = 2.30 eV, E_{gNG} = 1.82 eV, $m_c = 2\ m_0$, and τ_{nonrad} = 1 ns; (b) E_{gWG} = 2.30 eV, E_{gNG} = 1.82 eV, $m_c = 0.3\ m_0$, and τ_{nonrad} = 10 ns; (c) E_{gWG} = 2.04 eV, E_{gNG} = 1.52 eV, $m_c = 0.3\ m_0$, and τ_{nonrad} = 10 ns.

The optimal E_g values for the other reactors are summarized in Fig. S5. They also narrow with decreasing m_c and increasing τ_{nonrad}. Thus, J_{sup}, η_{H2}, and η_{CO} improve, as shown in Fig. 6.

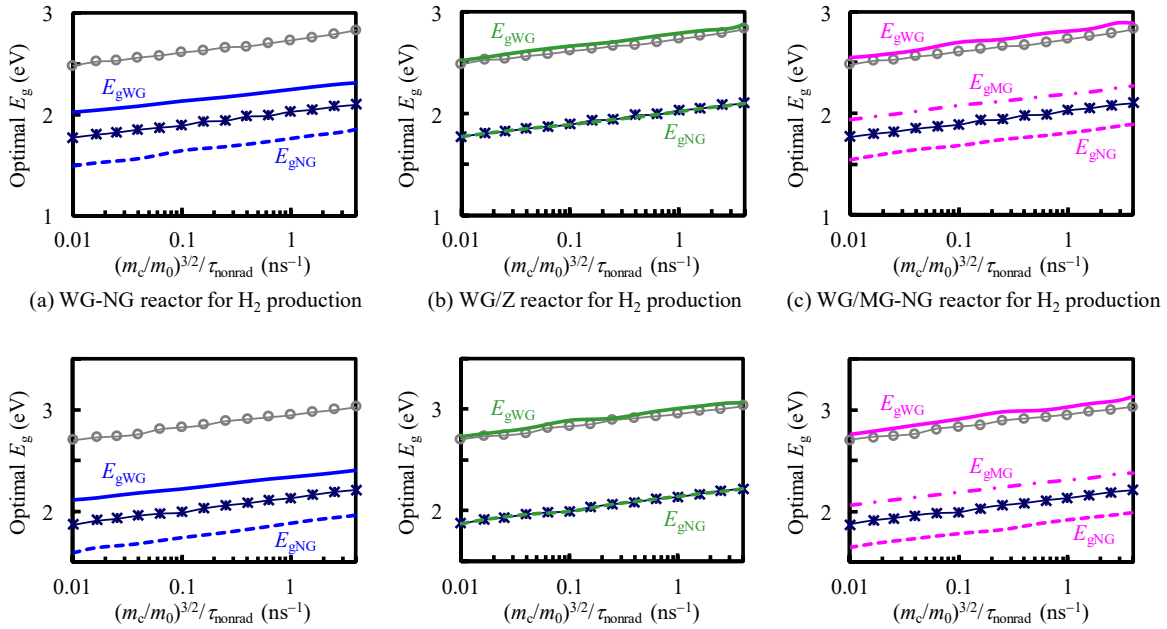

(a) WG-NG reactor for H_2 production (b) WG/Z reactor for H_2 production (c) WG/MG-NG reactor for H_2 production

(d) WG-NG reactor for CO production (e) WG/Z reactor for CO production (f) WG/MG-NG reactor for CO production

Fig. S5 Impacts of the carrier effective mass (m_c) and nonradiative recombination lifetime (τ_{nonrad}) on the optimal E_g values of the photocatalysts used in the spectrum-splitting reactors. The values for the single-material reactors (gray open circles) and conventional Z-scheme reactors (dark blue asterisks) are also shown for comparison. (a)–(c) H_2 production ($\Delta\mu_{op}$ = 1.6 eV) and (d)–(f) CO production ($\Delta\mu_{op}$ = 1.8 eV). ΔG = 0.2 eV and w = 4 μm are adopted.

As depicted in Fig. 7, J_{sup}, η_{H2}, and η_{CO} decrease with increasing ΔG. The E_g values optimized for each ΔG are plotted in Fig. S6. The N_{abs} and N_{gen} values of the two kinds of the photocatalysts involved in the two-step excitation decrease with increasing ΔG, because the increase in the summation of the two E_g values is approximately the same as the increase in ΔG. For example, the optimal values in the WG-NG reactor for H_2 production (Fig. S6(a)) are E_{gWG} = 2.30 eV and E_{gNG} = 1.82 eV at ΔG = 0.2 eV, whereas they increase to E_{gWG} = 2.49 eV and E_{gNG} = 2.06 eV (the summation increases by 0.43 eV) at ΔG = 0.6 eV. On the other hand, ΔG = 0 eV is feasible for the WG/Z reactor when an all-solid-state Z-scheme cell is employed, leading to a narrower E_{gNG} and a resultant larger J_{sup} as shown in Fig. 7.

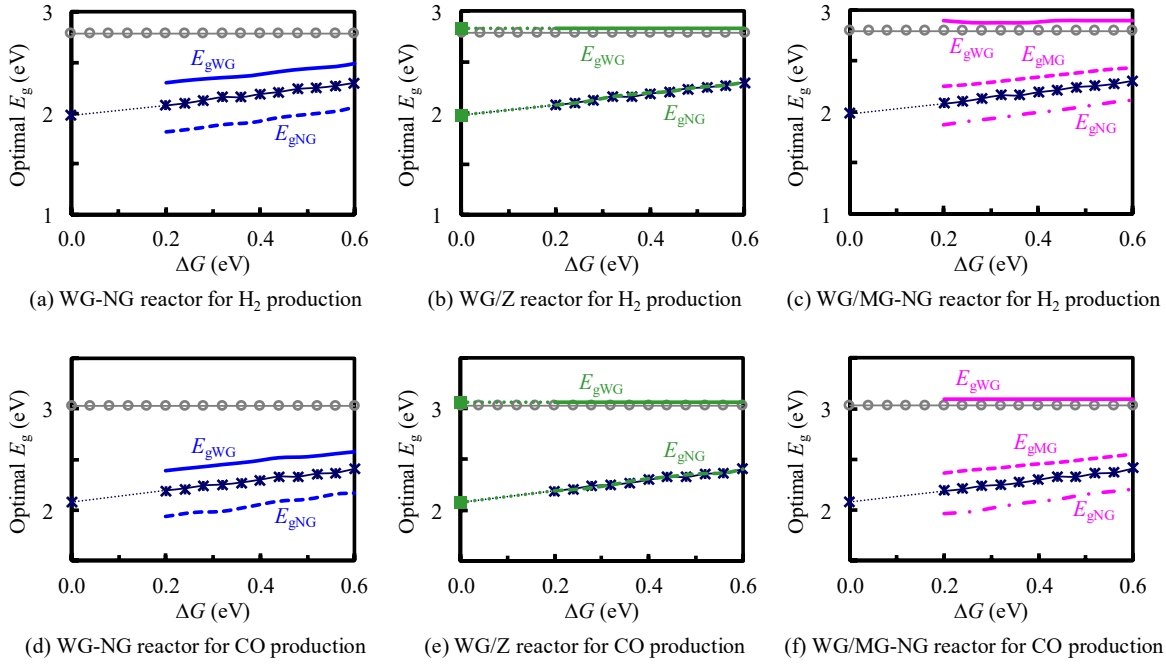

(a) WG-NG reactor for H_2 production (b) WG/Z reactor for H_2 production (c) WG/MG-NG reactor for H_2 production

(d) WG-NG reactor for CO production (e) WG/Z reactor for CO production (f) WG/MG-NG reactor for CO production

Fig. S6 Impacts of the driving force for electron transfer via the redox mediators (ΔG) on the optimal E_g values of the photocatalysts used in the spectrum-splitting reactors. The values for the single-material reactors (gray open circles) and conventional Z-scheme reactors (dark blue asterisks) are also shown for comparison. (a)–(c) H_2 production ($\Delta\mu_{op}$ = 1.6 eV), and (d)–(f) CO production ($\Delta\mu_{op}$ = 1.8 eV). m_c = 2 m_0, τ_{nonrad} = 1 ns and w = 4 μm are adopted. ΔG = 0.2 eV is the lower limit for the WG-MG and WG/MG-NG reactors using two-compartment cells, whereas ΔG = 0 eV is feasible for the Z-scheme and WG/Z (solid green squares) reactors when all-solid-state Z-scheme cells are employed.

S.2 Impacts of solar spectrum variation

The J_{sup} values of the reactors optimized for the AM 1.5G spectrum change when these reactors operate under different solar spectra, as depicted in Fig. 8. Figure S7 shows the E_g values of the photocatalysts used in the reactors optimized for H_2 production ($\Delta\mu_{op}$ = 1.6 eV) under the AM 1.5G illumination, in addition to the spectral solar photon flux ($n_{sun}(\hbar\omega)$) [1, 2].

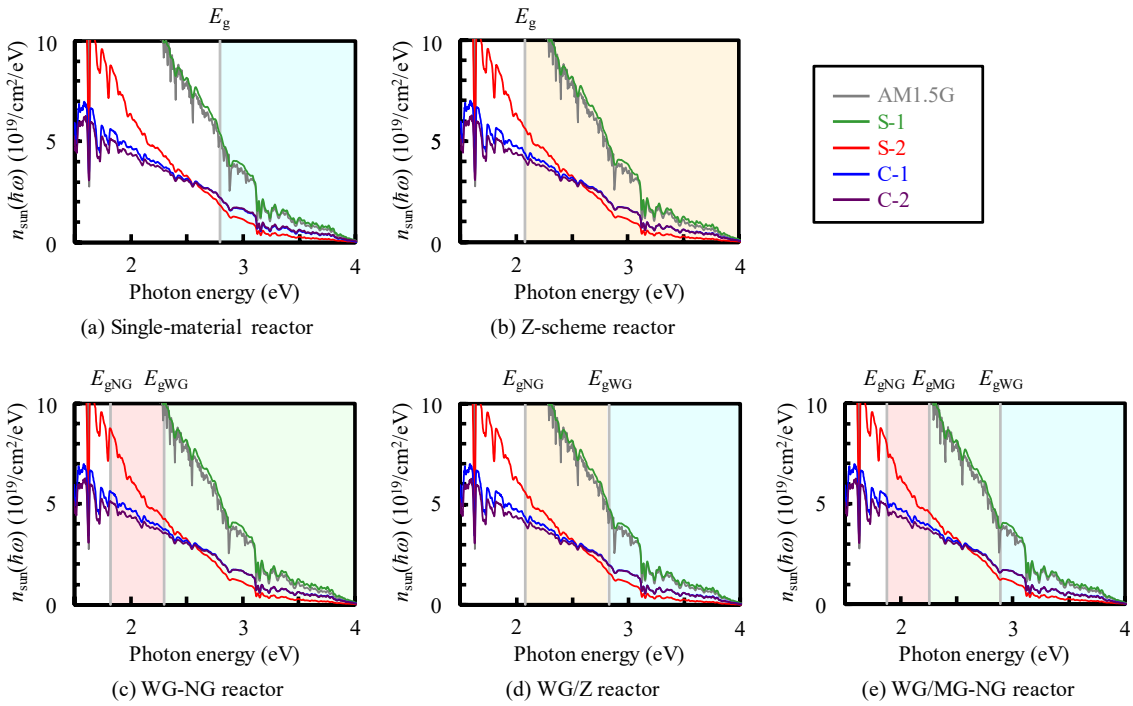

Fig. S7 Spectral photon fluxes ($n_{sun}(\hbar\omega)$) of the AM1.5G and measured solar spectra [1, 2], and E_g values of the photocatalysts used in the reactors optimized for H_2 production ($\Delta\mu_{op}$ = 1.6 eV) under the AM1.5G illumination.

The J_{sup} values of the single-material and Z-scheme reactors are directly related to $n_{sun}(\hbar\omega)$ at higher $\hbar\omega$ than E_g. Therefore, the magnitude relations among the J_{sup} values under the different spectra reflect $n_{sun}(\hbar\omega)$ shown in Figs. S7(a) and S7(b), respectively, integrated from E_g to infinity, i.e., $N_{gen}(E_g, \infty)$ (see eq (2)). The optimal E_g for the single-material reactor is 2.79 eV. The S-1 spectrum exhibits the largest $n_{sun}(\hbar\omega)$ in this range, followed by AM 1.5G, C-1, C-2, and S-2 in descending order, and the order of the J_{sup} values is the same. As for the conventional Z-scheme reactor, the S-2 includes more photons than the C-1 and C-2 in the range from the optimal E_g of 2.08 eV to 2.55 eV, whereas the magnitude relation of $n_{sun}(\hbar\omega)$ reverses in the higher-energy range. This reduces the differences in the $\hbar\omega$-integrated values, i.e., $N_{gen}(E_g, \infty)$ and resultant J_{sup}

values among these three spectra.

As for the spectrum-splitting WG/Z reactor, J_{sup} is similarly affected by the spectrum variation. However, $\eta_{sun}(\hbar\omega)$ in the absorption range of the Z-scheme cell on the backside (2.08–2.83 eV) should be integrated with a weighting factor of 1/2 because two photons are consumed for a single carrier supply.

On the other hand, J_{sup} of the WG-NG reactor is determined by the smaller one of the N_{abs} values of the WG and NG compartments, i.e., $N_{gen}(E_{gWG}, \infty)$ and $N_{gen}(E_{gNG}, E_{gWG})$. This changes the magnitude relation of the J_{sup} values under the different spectra from that for the three configurations described above. The C-1 and C-2 exhibit larger $\eta_{sun}(\hbar\omega)$ than the S-2 in the most of the absorption range of the WG-PCs over 2.30 eV. By contrast, $\eta_{sun}(\hbar\omega)$ in the S-2 is larger in the NG-PC absorption range of 1.82–2.30 eV. The latter effect surpasses the former, and consequently J_{sup} under the S-2 is slightly larger than those under the C-1 and C2. As for the WG/MG-NG reactor, the two factors for the single-material reactor and WG-NG reactor compete mutually, and as a result, the three J_{sup} values under the S-2, C-1, and C-2 are close to each other.

S.3 Impacts of the diameter and total volume on scattering and absorption by the photocatalyst particles

Figure S8 shows the dependence of the scattering cross section (C_{sca}) and absorption cross section (C_{abs}) on the diameter of the photocatalyst particle (d) suspended in water. In addition to an increase in C_{sca} with d, C_{sca}/S and C_{sca}/V that are the values normalized by the geometric cross section, S, and volume, V, respectively, also increase. By contrast, C_{abs}/V scarcely changes. This means that the scattering function enhances with increasing d at a constant w whereas the absorption function does not change, because the mean-free passes for the scattering and absorption are $\lambda_{sca} = (w C_{sca}/V)^{-1}$ and $\lambda_{abs} = (w C_{abs}/V)^{-1}$, respectively (see eqs (16) and (17)). As a result, the absorptivity for the high-energy photons lowers and instead the reflectivity increases with increasing d, as shown in Fig. 9(a).

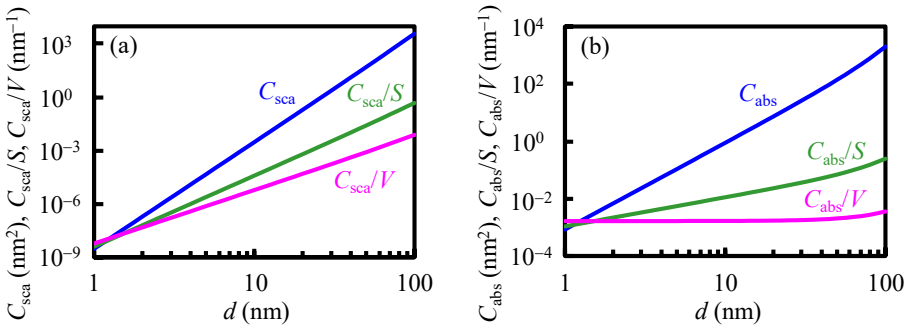

Fig. S8 (a) Scattering cross section (C_{sca}) of the photocatalyst particle suspended in water as functions of the diameter (d), and the normalized values by the geometric cross section (S) and volume (V). (b) Absorption cross section (C_{sca}) and normalized values. Photon energy is 2.40 eV that is higher than the optimal E_{gWG} = 2.30 eV of the WG-PCs used in the WG-NG reactor for H_2 production ($\Delta\mu_{op}$ = 1.6 eV) by 0.10 eV. Complex refractive index of the WG-PCs of $n + ik = 3.0 + i\,0.17$, and refractive index of water of 1.33 are adopted (see Section 4.4).

In the present model described in Section 3.4, the incident light is scattered sequentially by the photocatalyst particles with no interaction between the particles. This independent scattering model has been empirically found to be applicable when the following relation is fulfilled [3]:

$$\left(\frac{0.9047}{f^{1/3}} - 1\right)\frac{nd}{\lambda} > 0.5 \qquad \text{(S1)}$$

where f is the volume fraction of the particles, n the refractive index of the medium (n = 1.33 for water), and λ the wavelength of light. When the thickness of the WG

compartment is 1 cm, w = 1–6 μm adopted in Fig. 10 correspond to f = 1–6×10^{-4}. The left-side value of eq (S1) ranges from 0.91 (w = 1 μm) to 0.48 (w = 6 μm) under the present condition of λ = 540 nm (photon energy 2.30 eV) and d = 20 nm. Therefore, the independent scattering model provides accurate values except the case when w is close to 6 μm. On the other hand, the relative error of the model increases when d decreases at a constant w because the distance between the neighboring particles shortens [4]. Nevertheless, the results shown in Fig. 9 hold; both the absorptivity for the high-energy photons and transmissivity for the low-energy photons are close to unity at d < 10 nm, because C_{sca}/V is extremely small whereas C_{abs}/V is almost constant independent of d as is clear from Fig. S8.

References

[1] Solar Radiation Database, New Energy and Industrial Technology Development Organization (NEDO), https://www.nedo.go.jp/library/nissharyou.html. (accessed January 2021).

[2] Reference Solar Spectral Irradiance: Air Mass 1.5, National Renewable Energy Laboratory, https://rredc.nrel.gov/solar/spectra/am1.5/. (accessed January 2021).

[3] C. L. Tien, and B. L. Drolen, Thermal radiation in particulate media with dependent and independent scattering, *Ann. Rev. Heat Transf.*, 1987, **1**, 1–32.

[4] T. Galy, D. Huang, and L. Pilon, Revisiting independent versus dependent scattering regimes in suspensions or aggregates of spherical particles, *J. Quant. Spectrosc. Radiat. Transf.*, 2020, **246**, 106924.